

Cryogenic cave minerals recorded 1889 CE melt event in northeast Greenland

Anika Donner¹, Paul Töchterle¹, Christoph Spötl¹, Irka Hajdas², Xianglei Li³, R. Lawrence Edwards⁴, Gina
5 E. Moseley¹

¹Institute of Geology, University of Innsbruck, Austria

²Laboratory of Ion Beam Physics, ETH Zurich, Switzerland

³Institute of Earth Environment, Chinese Academy of Sciences, China

⁴Department of Earth Sciences, University of Minnesota, USA

10 *Correspondence to:* Anika Donner (anika.donner@uibk.ac.at)

Abstract. The investigation of cryogenic cave minerals (CCMs) has developed in recent decades to be a particularly valuable proxy for palaeo-permafrost reconstruction. Due to difficulties, however, in obtaining reliable chronologies with the so-called “fine” form of these minerals, such studies have thus far utilised the “coarse” form. In this study, we successfully investigate the northernmost-known deposit of fine-grained cryogenic cave minerals (CCMs), which are situated in Cove Cave (Greenlandic translation: Eqik Qaarusussuaq), a low-elevation permafrost cave in northeast Greenland (80° N). The Cove Cave CCMs display a complex mineralogy that consists of fine-grained cryogenic cave carbonates (CCC_{fine}) as well as sulphate minerals (gypsum, eugsterite, mirabilite, and löweite). ~~In comparison to CCC_{fine} from the mid-latitudes, positive $\delta^{13}\text{C}$ values (7.0 to 11.4‰) recorded in Cove Cave are similar. In contrast, Cove Cave CCC_{fine} $\delta^{18}\text{O}$ values are ca. 8 to 16‰ lower. Furthermore, despite~~ Until now, previous attempts to date CCC_{fine} dating efforts, fine-grained CCMs have been ~~ing~~ unsuccessful, however, here we demonstrate that precise dating is possible with both isochron-based $^{230}\text{Th}/\text{U}$ dating and ^{14}C dating if the dead carbon fraction is reliably known.

The dating result (65 ± 17 a BP; 1885 ± 17 CE) shows that the Cove Cave CCMs formed during the late Little Ice Age, a time interval characterised by cold temperatures and abundant permafrost in northeast Greenland, making water infiltration into Cove Cave dependent on water amount and latent heat. We relate the CCM formation to a combination of black carbon deposition and anomalously high temperatures, which ~~occurred over a few days, in the summer of 1889 CE. Such extreme conditions~~ led to widespread melting over large areas of the Greenland ice sheet in the course of a few days. We propose that the anomalous ~~(weather)~~ conditions of 1889 CE also affected northeast Greenland, where the enhanced melting of a local ice cap resulted in water entering the cave and rapidly freezing. While ~~CCC_{fine} calcite~~ and gypsum likely precipitated concurrently with freezing, the origin of the other sulphate minerals might not be purely cryogenic but could be linked to subsequent sublimation of this ice accumulation in the a very dry cave environment.

30

1 Introduction

In recent decades, cryogenic cave carbonates (CCCs), a type of speleothem associated with the formation of cave ice, have become a valuable tool for tracking evidence of past permafrost presence, particularly in the mid-latitudes in either low-elevation temperate locations (e.g., central Europe; Richter et al., 2018; Žák et al., 2012) or high-elevation periglacial environments (Bartolomé et al., 2015; Luetscher et al., 2013; Spötl et al., 2021; Spötl and Cheng, 2014). In contrast, investigations into CCCs from high-latitude caves are rare with the exception of a few studies from northern Yukon, Canada (Clark and Lauriol, 1992; Lauriol et al., 1988; Lauriol and Clark, 1993).

The presently accepted mechanism for CCC formation is precipitation from freezing karst water (Žák et al., 2012). There are two types of CCCs which are commonly differentiated by grainsize (ca. 1 mm; Žák et al., 2018), resulting in the terms coarse- and fine-grained CCCs (CCC_{coarse} and CCC_{fine}), despite the fact that the isotopic composition is the main diagnostic feature (a result of open vs. closed system precipitation; Luetscher et al., 2013). CCC_{coarse} are typically found in micro-climatically stable environments of cave interiors, where they precipitate in slowly freezing pools of water carved into cave ice deposits by drip water, making them a useful proxy for the reconstruction of palaeo-permafrost (i.e., CCC_{coarse} = palaeo-permafrost) as well as negative cave temperatures close to 0°C (Žák et al., 2018). In contrast, CCC_{fine} precipitate from a rapidly freezing film of water on top of cave ice and are commonly found in well ventilated caves and/or near cave entrances and thus may be related to local thermal anomalies, causing them to be unsuitable for permafrost reconstruction rather than regional permafrost (Žák et al., 2012). In addition to ~~CCC~~ carbonates, other minerals are also known to form cryogenically in caves, e.g., gypsum and other sulphate minerals, collectively referred to as cryogenic cave minerals (CCMs; Žák et al., 2018). In this paper, we follow the approach of

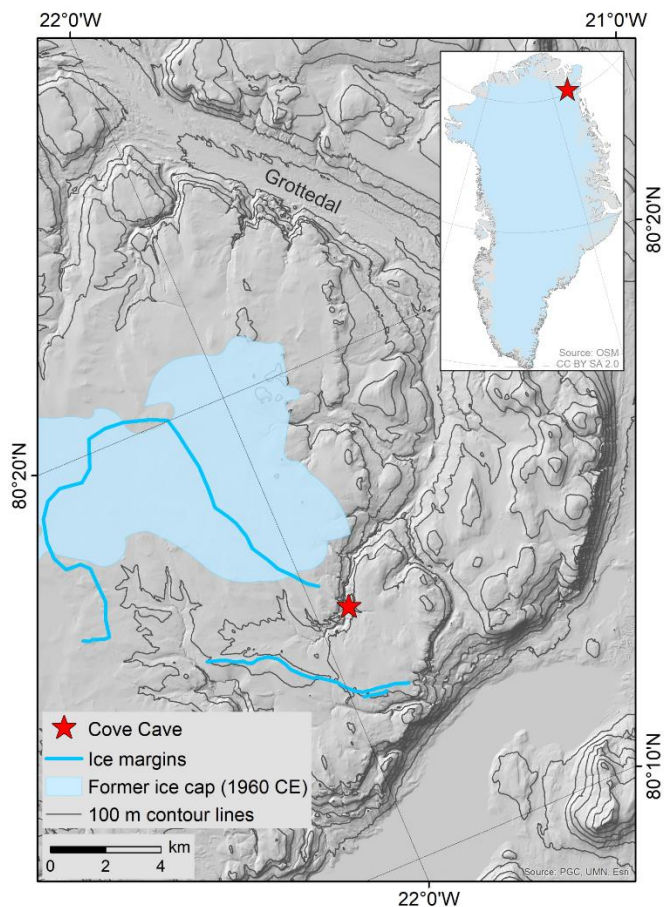
Žák et al. (2018) and use the term (fine-grained) CCMs to describe our samples, at times distinguishing the carbonate and sulphate fractions, whilst also comparing them to the CCM subtypes CCC_{coarse} and CCC_{fine}, -which from previous studies mostly focussed on.

CCC_{coarse} can be radiometrically dated using standard ²³⁰Th/U techniques (e.g., Koltai et al., 2021; Luetscher et al., 2013; Spötl et al., 2021; Žák et al., 2012), although the accuracy of ²³⁰Th/U ages using standard evaluation procedures has been recently called into question by showing that the conventionally used correction factors for detrital Th contamination are not universally applicable to CCC_{coarse} samples (Töchterle et al., 2022). Dating of CCC_{fine}, on the other hand, has proven to be a difficult task. ¹⁴C dating of CCC_{fine} suffers from large uncertainties associated with estimating the initial radiocarbon activity and the dead carbon fraction (DCF); (Lauriol and Clark, 1993), whereas ²³⁰Th/U dating has been hindered by poor age precision due to very high detrital thorium contamination, which is particularly challenging in young (i.e., late Holocene) samples (Spötl, 2008; Spötl and Cheng, 2014). Due to these unsuccessful dating efforts, the potential of CCC_{fine} as a palaeoclimate archive has yet to be realised.

In this study, we investigate fine-grained CCMs from a low-elevation permafrost cave (Cove Cave (unofficial name); Eqik Qaarusussuaq (Greenlandic)) in northeast Greenland; Cove Cave is currently the northernmost-known cave containing cryogenic mineral deposits, which and is located within a climatically highly sensitive region adjacent to the Greenland ice sheet (Bintanja and Krikken, 2016; Bintanja and Selten, 2014; Shepherd, 2016). This paper aims to: i) extend the existing knowledge on morphology, mineralogy, and stable isotopic composition of fine-grained high-latitude CCMs; ii) constrain the age of fine-grained CCMs (and CCC_{fine}) using ²³⁰Th/U and ¹⁴C dating methods; and iii) ascertain the circumstances of CCM formation at this location.

2 Study Site

Cove Cave (80.25° N, 21.93° W) is located in a small tributary valley to a steep-sided canyon on Kronprins Christian Land in northeast Greenland (Fig. 1; Moseley et al., 2020). The Silurian limestones and dolostones in this area host numerous solution caves (Smith and Rasmussen, 2020), some of which were first discovered in 1960 (Davies and Krinsley, 1960), followed by more cave discoveries during three subsequent caving expeditions (Loubière, 1987; Moseley et al., 2020). The area is located ca. 35 km from the coast (eastwards) and ca. 60 km from the margin of the Greenland ice sheet (south-westwards). It is characterised by an arid climate (ca. 200 mm a⁻¹; Schuster et al., 2021), permanently frozen ground, sparse soil and vegetation cover, and permafrost landforms (Moseley et al., 2020). Under contemporary climatic conditions, common speleothems (i.e., stalactites, stalagmites, and flowstones) can therefore not form in the caves of the area due to the lack of water infiltration. Weather stations or long-term weather observations are absent in the area, however, mean annual air temperatures at the nearest weather station s on the ice sheet (KPC_L PROMICE weather station, 07/2008–12/2021; ca. 70 km away; Fausto et al., 2019; van As et al., 2011) and near the coast (Station Nord, 1991–2020; ca. 180 km away; Danmarks Meteorologiske Institut, 2022) are -13.5°C and -15.1°C, respectively. Compared to these two stations, a more continental climate with warmer summer temperatures is expected for the study site (Donner et al., 2020). In 1960 and 1983, a small ice cap was present on the plateau in close vicinity to Cove Cave but this has since melted (Fig. 1, light blue polygon; Davies and Krinsley, 1960; Loubière, 1987; Moseley et al., 2020; Moseley et al., 2021). Elsewhere in the area, local plateaus are now ice free in summer (Moseley et al., 2021), though there is ample geomorphological evidence that ice caps were present in the past (Fig. 1, blue lines; Sole et al., 2020), which might have covered the plateau above Cove Cave.



85

Figure 1: Location of Cove Cave in a tributary valley of the larger Grottedal valley in northeast Greenland (map insert: Geofabrik and OpenStreetMap Contributors, 2018). The cave is located close to margins of former ice caps. The most recent ice cap was mapped in 1960 ([light blue polygon](#); Davies and Krinsley, 1960), still existed in 1983 (Loubière, 1987) and disappeared before 2019 (Moseley et al., 2020). Geomorphological evidence of ice margins indicate the former presence of additional ice caps, which have not been dated ([blue lines](#); Sole et al., 2020).

90

Cove Cave consists of a 103 m long, gently dipping phreatic passage, making it currently the longest explored cave in Greenland (Fig. 2; Moseley et al., 2020). The cave hosts both CCMs and inactive flowstones ([i.e., without active water supply](#)), the latter indicating at least one phase of warmer and wetter climate in the past. The cave entrance is located 660 m above sea level with a rock overburden of ca. 25 m. Inside the entrance area, an ice pond, ice stalagmites, and hoar frost have been observed during a visit in summer (Moseley et al., 2020). Beyond the entrance area, the cave is devoid of ice. Flowstone drapes the walls of a vadose canyon and broken angular flowstone blocks, likely shattered by freeze–thaw processes, are scattered on the floor (Moseley et al., 2020). Accumulations of CCMs lie on the shattered flowstone blocks in an area ca. 3 x 1 m. At this location, an air temperature of -14.7°C was measured in July 2019 (Fig. 2), while the outside air temperatures reached up to 18°C (Donner et al., 2020; Moseley et al., 2020). Measurements of relative humidity only exist for other parts of the cave where temperatures were above -10°C, reaching values as low as 39 % at floor level (Barton et al., 2020). It can therefore be inferred that the relative humidity in colder parts of the cave must also be [rather](#)-low. Cold air has less capacity to hold moisture and incoming air loses much of its humidity by resublimation, creating hoar frost on the walls close to the cave entrance (Barton et al., 2020; Lauriol et al., 1988). Deeper inside the cave, flowstone deposits block a ca. 5 m deep vadose slot, at the bottom of which cave air temperatures reached -17.1°C (Barton et al., 2020; Moseley et al., 2020). The cause of these low temperatures is likely density-driven flow of very cold winter air into this descending single-entrance cave. During summer, a stable air stratification inside this cold trap prevents advection of warm outside air into the cave (Barton et al., 2020).

95

100

105

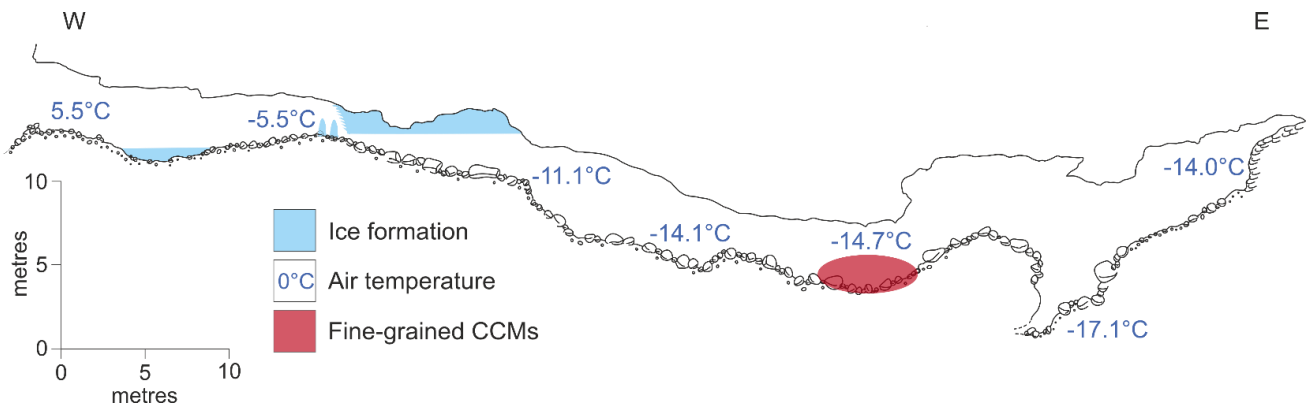


Figure 2: Longitudinal section of Cove Cave. Ice formations such as an ice pond, ice stalagmites, and hoar frost are only present in the first third of the cave. Beyond, air temperatures are much lower. CCMs were found ca. 65 m behind the entrance (adapted from Moseley et al., 2020).

110

3 Materials and Methods

3.1 Sampling and sample preparation

Sampling took place in four different spots within the 3 x 1 m accumulation of CCMs in July 2019. Four samples (KC19CCC-1, KC19CCC-2, KC19CCC-3, and KC19CCC-4) were picked up with a knife, wrapped in aluminium foil, and stored in plastic containers. There were no obvious visual differences between the samples during collection. During sampling, disturbance to the overall appearance of the CCM accumulation and Cove Cave was kept to a minimum.

In the lab, the samples were homogenised and transferred to glass vials in a laminar-flow hood. For all subsequent analyses, macroscopic contaminants (e.g., pieces of bedrock or insect remains) were removed under a binocular microscope. To aid the calculation of the DCF, four artificial mixtures ranging from 100 wt.-% CCM fraction to 100 wt.-% non-CCM fraction were produced from KC19CCC-4 by splitting the sample into the different mineral fractions and mixing the relative amounts. Overall, analysis options and the reproducibility of analyses were limited by the available sample amount.

3.2 Mineralogy and crystal morphology

A Bruker D8 Discover X-ray diffractometer (XRD) in Bragg-Brentano geometry equipped with a Cu target and a LYNXEYE detector was used to analyse the mineralogical composition of the samples (Cu-K_α radiation: 1.5406 Å; 2θ range: 8-45°). Further, a HORIBA JOBIN-YVON LabRam-HR800 spectrometer, excited by a frequency-doubled Nd-YAG laser (100 mW, 532 nm), was used for the in situ determination of the mineralogy of individual grains at a resolution of ca. 5 μm.

A Keyence VHX 6000 digital microscope was used to examine the morphology of the CCMs. To study the fine fraction, a field-emission scanning electron microscope (SEM) operating at 10 kV accelerating voltage was utilised (DSM 982 Gemini, Zeiss).

130

3.3 Stable isotope analysis

Fourteen aliquots of 0.15 to 0.7 mg of the carbonate fraction were taken from the four samples and their carbon and oxygen stable isotopic composition was analysed using a Thermo Fisher Delta V Plus isotope ratio mass spectrometer coupled with a Gasbench II (Spötl and Vennemann, 2003), yielding a long-term precision of ± 0.08 ‰ for $\delta^{18}\text{O}$ and ± 0.06 ‰ (1σ) for $\delta^{13}\text{C}$ (Spötl, 2011). For comparison, carbon and oxygen isotope data from inactive common speleothems in the study area (a few square km) were included. The common speleothems were collected in several caves, including Cove Cave. All results were calibrated against international standards and reported relative to the Vienna Pee Dee Belemnite (VPDB) standard.

140 3.4 Radioisotope dating

3.4.1 $^{230}\text{Th}/\text{U}$ disequilibrium dating and isochron construction

For $^{230}\text{Th}/\text{U}$ disequilibrium dating of the carbonate fraction, 20 mg aliquots from each of the four samples were picked in a laminar-flow hood. Dating, including chemical preparation and multi-collector inductively coupled mass spectrometry, was carried out at the Trace Metal Isotope Geochemistry Laboratory at the University of Minnesota following Edwards et al. (1987) and Shen et al. (2012). Ages are reported in years before 1950 CE (a BP) with 2σ uncertainties. Additionally, $\delta^{234}\text{U}$ values of inactive common speleothems from Cove Cave were included in this study.

An isochron using maximum likelihood regression (Ludwig and Titterton, 1994) was constructed in IsoplotR (Vermeesch, 2018) using the ^{238}U -normalised activities of ^{234}U , ^{230}Th and ^{232}Th . Additionally, the initial $^{230}\text{Th}/^{232}\text{Th}$ activity ratio was ascertained and applied to the detrital Th correction of the individual ages as a reliability test of the derived isochron values in order to establish whether there was one or multiple sources of detrital ^{230}Th (Dorale et al., 2004). Ages are reported in years BP with 2σ measurement uncertainties.

3.4.2 Radiocarbon dating and calculation of DCF

Eight aliquots of 16–31 mg were taken from the samples, including artificial mixtures. All eight aliquots were analysed with a MICADAS accelerator mass spectrometer (AMS) in the Laboratory of Ion Beam Physics at ETH Zurich (Synal et al., 2007). Radiocarbon values are reported as conventional radiocarbon ages before present $\pm 1\sigma$ (BP) (Stuiver and Polach, 1977) and as fraction modern $\pm 1\sigma$ ($F^{14}\text{C}$) (Reimer et al., 2004; Reimer et al., 2020) relative to 95 % of the secondary standard HOx2 (Hajdas et al., 2021).

The DCF calculation is based on the equation given by Genty and Massault (1997), using the measured $F^{14}\text{C}$ of the sample ($F^{14}\text{C}_{\text{sample}}$) in relation to the atmospheric $F^{14}\text{C}$ at the time of formation ($F^{14}\text{C}_{\text{atm}}$), which was obtained by the corrected $^{230}\text{Th}/\text{U}$ age and the IntCal20 calibration curve (Reimer et al., 2020; Eq. 1):

$$DCF = \left(1 - \frac{F^{14}\text{C}_{\text{sample}}}{F^{14}\text{C}_{\text{atm}}}\right) \times 100 \% \quad (1)$$

The radiocarbon ages were then corrected for the corresponding DCFs, resulting in a radiocarbon age ± 2 standard errors for 0 % DCF, calculated by linear approximation and calibrated against IntCal20 (cal BP) (Reimer et al., 2020) using OxCal 4.4 (Bronk Ramsey, 2009).

4 Results

4.1 Mineralogical composition and particle morphology

All four samples show a complex mineralogy and a range of particle morphologies that consist of crystal aggregates and single crystals of variable size. The aggregates range from 50 to 400 μm in diameter, rarely exceeding 500 μm , while individual crystals range from 1 μm to a few tens of micrometres. Brownish sub-micrometric crystals dominate sample KC19CCC-1, which contains larger translucent and opaque white as well as brownish crystals and crystal aggregates (Fig. 3a). Sample KC19CCC-2 (Fig. 3b) is homogeneously white with opaque and translucent crystals/crystal aggregates. The other two samples (KC19CCC-3 and -4; Fig. 3c) are made up of larger white and brownish crystals/crystal aggregates and brownish sub-micrometric crystals resulting in a speckled appearance.

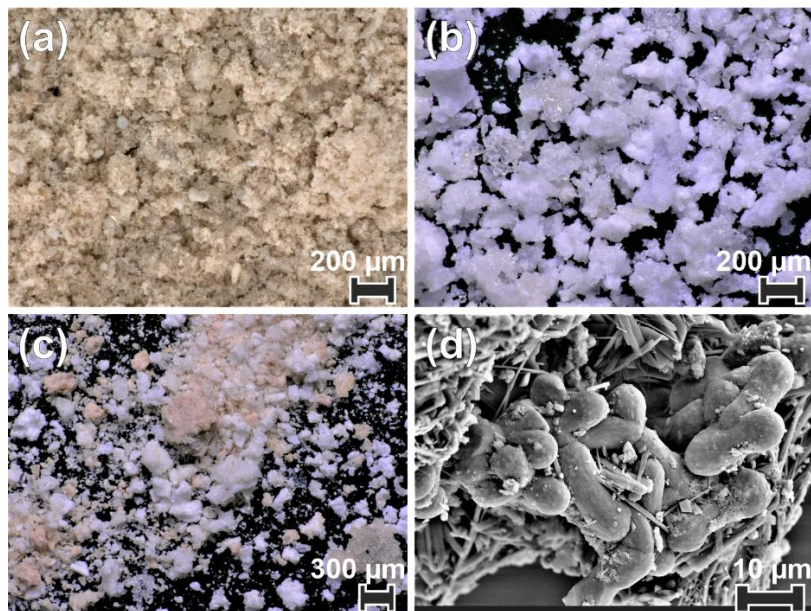


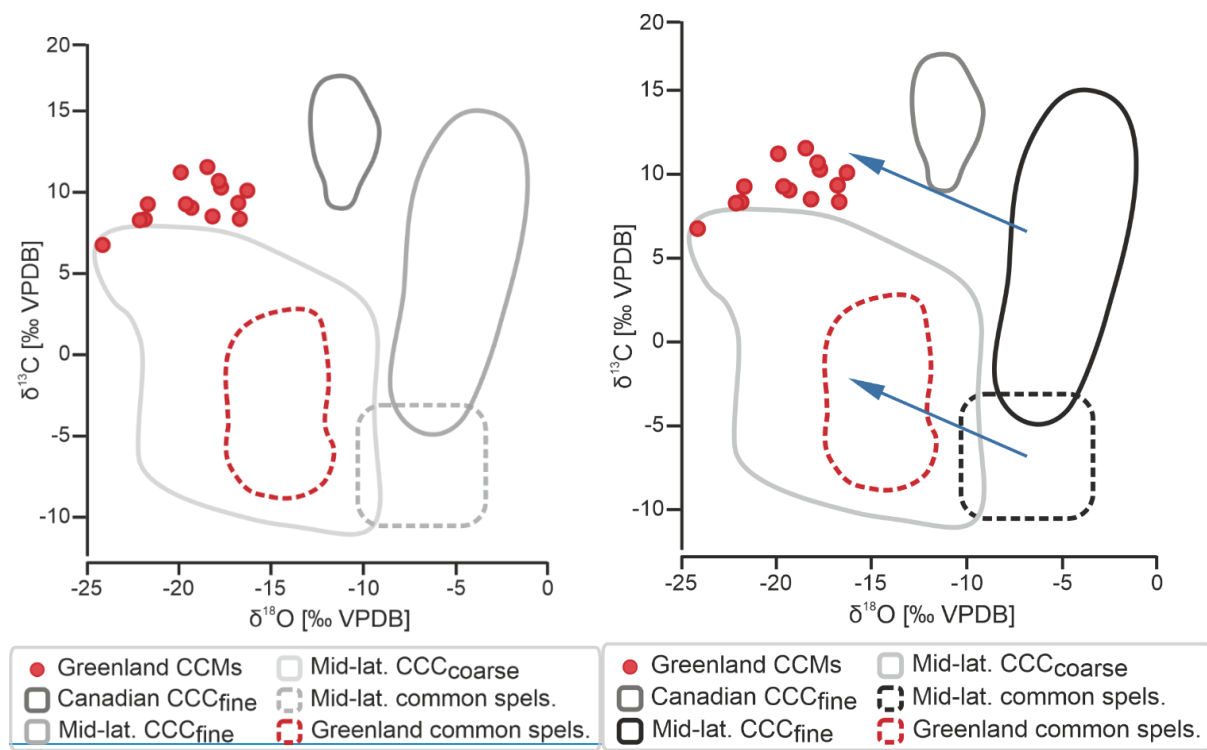
Figure 3: Optical (a–c) and SEM (d) images of the studied cryogenic samples. (a) Brownish very fine crystals ([quartz, potassium feldspar and traces of dolomite](#)~~unknown composition~~) intermixed with brownish crystal aggregates (calcite) and white/translucent single crystals made up of calcite, dolomite and gypsum (sample KC19CCC-1). (b) White calcite, gypsum, eugsterite, mirabilite, and löweite (sample KC19CCC-2). (c) Mixed white (calcite and sulphate minerals) ~~and~~ brownish (calcite) particles [and traces of quartz](#) (samples KC19CCC-3 and -4). (d) Intermixed dumbbell-shaped calcite and acicular sulphate minerals which are present in all samples.

XRD results ([see Appendix A](#)) show that the samples are mostly mixtures of calcite and the sulphate minerals gypsum ($\text{CaSO}_4 \cdot 2\text{H}_2\text{O}$), eugsterite ($\text{Na}_4\text{Ca}(\text{SO}_4)_3 \cdot 2\text{H}_2\text{O}$), löweite ($\text{Na}_{12}\text{Mg}_7(\text{SO}_4)_{13} \cdot 15\text{H}_2\text{O}$), and mirabilite ($\text{Na}_2\text{SO}_4 \cdot 10\text{H}_2\text{O}$). Sample KC19CCC-1 contains additional phases such as quartz, dolomite, and potassium feldspar, [while quartz is also present in samples KC19CCC-3 and -4.](#)

The CCMs contain a variety of crystal morphologies, comparable to the morphologies of $\text{CCC}_{\text{coarse}}$ (Žák et al., 2018), albeit of much smaller sizes. Predominant morphologies are spherulitic and acicular as well as aggregates of elongated prismatic crystals. Further, rhombic and dumbbell-shaped morphologies were observed. Optical microscopy combined with micro-Raman spectroscopy showed that calcite is mostly represented as translucent and opaque spherulitic crystals and crystal aggregates such as chains of different colours, whereas sulphate minerals mostly consist of white fibrous, acicular, and prismatic crystals. Raman spectroscopy and SEM imagery also showed that microcrystalline calcite and sulphate minerals are often intermixed (Fig. 3d).

4.2 Stable isotopes

The stable isotopic composition of the 14 aliquots ranges from -24.0 to -16.0 ‰ for $\delta^{18}\text{O}$ and from 7.0 to 11.4 ‰ for $\delta^{13}\text{C}$ (Fig. 4).
 195 The $\delta^{13}\text{C}$ values overlap with those of CCC_{fine} from mid-latitude caves (Žák et al., 2018). The $\delta^{18}\text{O}$ values, however, are significantly lower than values from mid-latitude CCC_{fine} and fall at the lower end of $\delta^{18}\text{O}$ values of mid-latitude $\text{CCC}_{\text{coarse}}$ (Žák et al., 2018).



200 **Figure 4:** Stable isotope composition of CCMs and common speleothems from northeast Greenland (this study) compared to CCC_{fine} from the Canadian Arctic circle (Clark and Lauriol, 1992) as well as CCC_{fine} and common speleothems from mid-latitude caves (Žák et al., 2018). The composition of $\text{CCC}_{\text{coarse}}$ from mid-latitude caves is also shown for comparison (Žák et al., 2018). Note the difference-latitudinal shift in $\delta^{18}\text{O}$ (blue arrows) that can be observed in both $\text{CCC}_{\text{fine}}/\text{CCMs}$ and common speleothems between the mid- and high-latitudes. in $\delta^{18}\text{O}$ between mid- and high latitude $\text{CCC}_{\text{fine}}/\text{CCMs}$ as well as between mid-latitude and Greenland common speleothems.

205 4.3 Radioisotope dating

Of the four $^{230}\text{Th}/\text{U}$ analyses, three yielded results (KC19CCC-2, KC19CCC-3, KC19CCC-4), while KC19CCC-1 contained too much detrital material to be analysed. Table 1 shows that the ^{238}U content is high (1113 ± 2 to 1278 ± 2 ng g^{-1}), as is the concentration of detrital thorium (indicated by the low $^{230}\text{Th}/^{232}\text{Th}$ activity ratio between 1.30 ± 0.04 and 3.89 ± 0.22). Uncorrected ages show a large range from 143 ± 11 to 7335 ± 48 a BP. However, the appearance of the sampling site and the presence of the same types of
 210 minerals in all samples suggest that they likely formed near-synchronously. The results yielded a highly correlated isochron ($R^2=0.998$), yet the maximum likelihood regression is heavily controlled by the sample with the highest analytical precision, which is the cleanest sample (KC19CCC-2). The high mean square of the weighted deviates (MSWD) of 69 indicates that the ages are over-dispersed compared to the stated analytical uncertainties and that an isochron accounting for this overdispersion is needed (Vermeesch, 2018). The resulting age of 65 ± 17 a BP agrees with the ages of two of the three samples (KC19CCC-2: 64 ± 12 a BP;
 215 KC19CCC-3: 172 ± 153 a BP) when corrected for detrital Th using the isochron-derived initial $^{230}\text{Th}/^{232}\text{Th}$ activity of 1.39 ± 0.006 (Fig. 5). The isochron-corrected age of KC19CCC-4 (353 ± 74 a BP) is, however, not in agreement with the other two samples

within dating uncertainty, thus suggesting multiple sources of initial ^{230}Th (e.g., Dorale et al., 2004). Nonetheless, this disagreement could also result from an underestimation of uncertainty by the maximum likelihood regression. The isochron-corrected $\delta^{234}\text{U}_{\text{initial}}$ is high for all three samples (1872 ± 3 to 2193 ± 5).

220

Table 1: Results of $^{230}\text{Th}/\text{U}$ disequilibrium dating.

Sample	^{238}U (ng g ⁻¹)	^{232}Th (ng g ⁻¹)	$^{230}\text{Th}/^{232}\text{Th}$ (activity)	$\delta^{234}\text{U}^*$ (measured)	$^{230}\text{Th}/^{238}\text{U}$ (activity)	Uncorrected ^{230}Th age (a)	$\delta^{234}\text{U}_{\text{initial}}$	Bulk-earth- corrected age (a BP)	Isochron- corrected age (a BP) [†]
KC19CCC-1	2658 ±6.5	2028±40.9	2.04±0.04	9±1.9	0.5139 ±0.0033				
KC19CCC-2	1236 ±3.0	6±0.1	3.89±0.22	2192±5.1	0.0062 ±0.0003	213±11	2193±5	97±34	64±12
KC19CCC-3	1113 ±1.9	480±9.6	1.30±0.04	1871±3.4	0.1898 ±0.0012	7405±48	1872±3	2918 ±3140	172±153
KC19CCC-4	1278 ±1.7	270±5.4	1.48±0.04	2058±2.9	0.1049 ±0.0007	3792±25	2058±3	1700 ±1433	353±74

All uncertainties are 2 σ .
U decay constants: $\lambda_{238} = 1.55125 \times 10^{-10}$ (Jaffey et al., 1971) and $\lambda_{234} = 2.82206 \times 10^{-6}$ (Cheng et al., 2013). Th decay constant: $\lambda_{230} = 9.1705 \times 10^{-6}$ (Cheng et al., 2013).
^{*} $\delta^{234}\text{U} = ((^{234}\text{U}/^{238}\text{U})_{\text{activity}} - 1) \times 1000$.
[†]corrected for detrital Th with initial $^{230}\text{Th}/^{232}\text{Th}$ activity of 1.39 ± 0.006

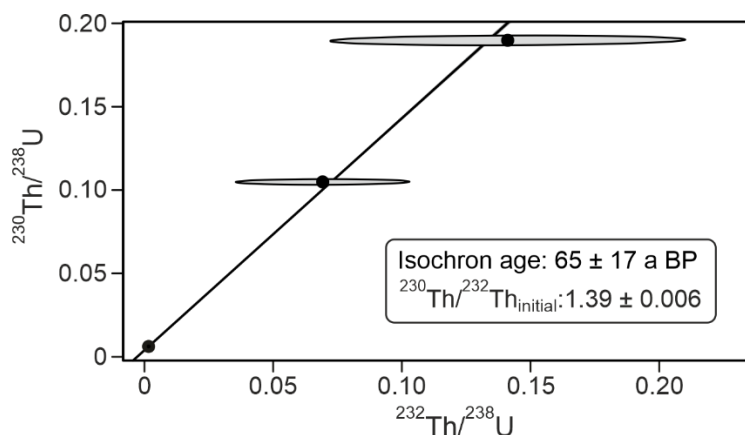


Figure 5: Maximum likelihood isochron with overdispersion based on the three $^{230}\text{Th}/\text{U}$ disequilibrium ages and calculated in IsoplotR (Vermeesch, 2018).

225

Conventional radiocarbon ages for the four untreated and four mixed aliquots range from 140 ± 27 to 2261 ± 74 a BP, with corresponding $F^{14}\text{C}$ values of 0.98 ± 0.003 to 0.06 ± 0.0006 (Table 1). When applying the radiocarbon method to speleothems the DCF needs to be determined (Genty and Massault, 1997) in order to correct for ^{14}C -free material from bedrock and/or soil (Bajo et al., 2017; Hajdas et al., 2021; Hua et al., 2012). The DCFs of all analysed aliquots range from 1.24 ± 0.50 to 93.67 ± 0.06 % (1 σ uncertainty). For the untreated aliquots, 96.2 % of variance in radiocarbon age can be explained by the DCF ($R^2=0.96$). When artificial mixtures are included, this value is lower ($R^2=0.88$), yet indicating that the artificial mixing was reasonably accurate. The radiocarbon age extrapolated to 0 % dead carbon by linear approximation is 2 ± 28 BP. Calibration using IntCal20 (Reimer et al., 2020) yielded three distinct peaks of calibrated ages: 36–73, 112–139 and 226–255 cal BP with respective probabilities of 37.8, 28.3 and 29.4 % (Fig. 6). The peak with the highest probability (36–73 BP) is in agreement with the $^{230}\text{Th}/\text{U}$ isochron age of 65 ± 17 a BP and provides the most likely timing for CCM formation. We attribute the other two peaks to a plateau of the calibration curve in this time interval.

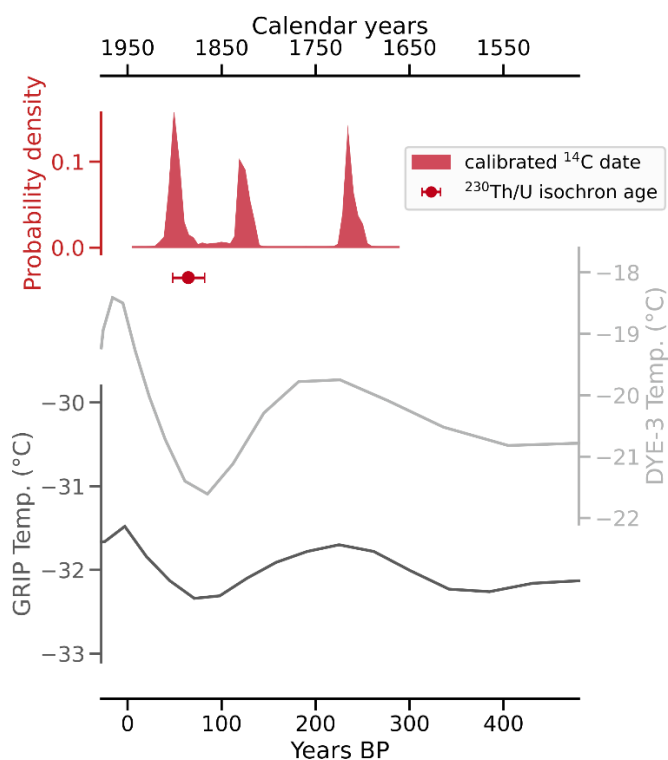
230

235

Table 2: Results of ^{14}C dating.

Sample	Lab code	^{14}C age (BP)		$F^{14}\text{C}$		$\delta^{13}\text{C}$ (‰)		DCF (%)	
KC19CCC-1	ETH-109243	12562 ±33		0.209	±0.0009	6.7	±1	79.00	±0.12
KC19CCC-2	ETH-109244	140 ±27		0.983	±0.0033	9.0	±1	1.24	±0.50
KC19CCC-3	ETH-109245	6337 ±35		0.454	±0.0020	3.1	±1	54.39	±0.26
KC19CCC-4	ETH-109246	1626 ±28		0.817	±0.0028	7.9	±1	17.92	±0.42
KC19CCC-4 100 % clean	ETH-112579	358 ±22		0.956	±0.0026	10.6	±1	3.95	±0.45
KC19CCC-4 90 % clean	ETH-112580	1758 ±23		0.803	±0.0023	9.5	±1	19.33	±0.38
KC19CCC-4 70 % clean	ETH-112581	2353 ±23		0.746	±0.0021	8.8	±1	25.05	±0.35
KC19CCC-4 0 % clean	ETH-112582	22261 ±74		0.063	±0.0006	2.2	±1	93.67	±0.06

All uncertainties are 1σ .



240 **Figure 6:** Calibrated and DCF-corrected ^{14}C dating results and $^{230}\text{Th}/\text{U}$ isochron age plotted against temperatures from two boreholes on the Greenland ice sheet (Dahl-Jensen et al., 1998) indicate that the Cove Cave CCMs formed during the late Little Ice Age. The two older peaks of the calibrated and corrected ^{14}C dates are likely the result of a plateau of the calibration curve at that time interval.

The dating results show that the CCMs formed during the late Little Ice Age, a period of relatively cold climate conditions and glacier advances, which in Greenland lasted between about 700 and 50 a BP (i.e., 1250 – 1900 CE; Kjær et al., 2022).

245

5 Discussion

5.1 Formation of CCMs

In carbonate-hosted caves, CCC_{fine} typically show a simple mineralogical composition, mostly consisting of calcite or, less commonly, other carbonate minerals such as aragonite, or mixtures thereof (Žák et al., 2018). In some caves, the occurrence of

250 non-carbonate minerals of cryogenic origin has been reported (Dublyansky et al., 2017; Žák et al., 2018). Cryogenic gypsum and, locally, other sulphate minerals are mostly known from caves hosted in gypsum rock (Kadebskaya and Tschaiikovskiy, 2015; Žák et al., 2018) but also from some limestone caves where the sulphate is derived from pyrite oxidation (Bartolomé et al., 2022; Dublyansky et al., 2017). Mirabilite is known from several caves where its existence has been tied to evaporative conditions (e.g., Audra and Nobécourt, 2013; Bieniok et al., 2011). Although it has been reported from cold caves (Harmon et al., 1983) and its
255 formation has been tied to preceding cryochemical processes, mirabilite was not regarded as primarily cryogenic in origin (Žák et al., 2018), and we are unaware of reports about cryogenically formed mirabilite in caves. Eugsterite is a rare sulphate mineral which has only been reported from two caves, Mammoth Cave, USA (White, 2017), and Chamois Cave, France (Audra and Nobécourt, 2013), where its formation is not related to cryogenic processes. Löweite has only rarely been described from volcanic caves (Hill and Forti, 1997).

260 In Cove Cave, the most likely source of dissolved sulphate, necessary for the precipitation of sulphate minerals, is finely disseminated pyrite in the dark-coloured Silurian limestones in which this cave developed (Smith and Rasmussen, 2020), whereas magnesium for löweite formation was likely sourced from dolostones in the area. In contrast the presence of sodium, which is needed for the minerals mirabilite, löweite, and eugsterite is more challenging to explain. One possibility is that, given the proximity to the coast, the Na is sourced from aerosols from the ocean and/or the sea ice surface, which has been recognised as a
265 dominant source for Na in coastal Arctic ice cores (Rhodes et al., 2018). The most probable source for the traces of dolomite is the host rock, while traces of quartz and potassium feldspar are, most likely, detrital material that entered the cave via water influx or aeolian transport.

The mode of formation (during freezing or sublimation) of the hydrated sulphate minerals must also be considered, especially with respect to whether their formation was synchronous with the precipitation of ~~CCC_{fine}~~the carbonate fraction. While careful
270 examination of SEM images yielded no conclusive evidence of coeval crystal growth. ~~T~~the high solubility of eugsterite, mirabilite, löweite, and to a lesser extent gypsum, can ~~however~~ be used to provide ~~such~~ insights. For instance, it is clear that the four sulphate minerals did not form prior to the influx of water and subsequent freezing, otherwise pre-existing soluble minerals would have been dissolved and/or washed away. Likewise, the high solubility of these sulphate minerals suggests that the ice in which the
~~CCC_{fine}~~cryogenic carbonates were embedded, did not melt but rather sublimesublimates, otherwise these delicate crystals would
275 not have been preserved. Furthermore, the cave section hosting the sampling site must have remained dry and ice-free since the formation of the CCMs. This also implies that the cave ventilation pattern at the time of formation was already similar to the present mode in this sag-type cave.

Based on the observation that the calcite and sulphate minerals were found intermixed, it seems likely that the formation of the sulphate minerals was associated with the formation of ~~CCC_{fine}~~the carbonate fraction, in the sense that both their formations were
280 triggered by the same event, and therefore took place near-synchronously. Whether this formation was cryogenic, or occurred during the subsequent sublimation of ice cannot be determined with certainty. A cryogenic formation of gypsum is likely, similar to the observed formation in other ice caves (see above; e.g., Žák et al., 2018) but the other sulphate minerals may have formed during the subsequent sublimation of ice after gypsum and ~~CCC_{fine}~~calcite had already formed.

285 5.2 Stable isotopes

The relatively high $\delta^{13}\text{C}$ (7.0-11.4 ‰) values of the Greenland CCMs are comparable to those of CCC_{fine} from the Canadian Arctic circle (Clark and Lauriol, 1992), however, the $\delta^{13}\text{C}$ of the Canadian samples reach higher values (up to 17 ‰). Nevertheless, these highly positive values reflect kinetic isotope fractionation as a result of rapid freezing and associated degassing of carbon dioxide (Lacelle et al., 2009).

290 The Cove Cave CCMs show highly depleted $\delta^{18}\text{O}$ (-24.0 to -16.0 ‰) values that are much lower than the $\delta^{18}\text{O}$ values of mid-latitude CCC_{fine} , and overlap with the lower range of $\delta^{18}\text{O}$ values of $\text{CCC}_{\text{coarse}}$ from mid-latitude caves (Fig. 4). Whilst $\text{CCC}_{\text{coarse}}$ $\delta^{18}\text{O}$ reflects closed-system freezing in small drip water pools in ice, the low values of the Greenland samples are largely related to the isotopically light meteoric precipitation in this high-Arctic setting. We are interpreting the low $\delta^{18}\text{O}$ values, which can be observed in Cove Cave CCMs, Cove Cave common speleothems (-17 to -13 ‰), and Canadian CCC_{fine} (although at a smaller
295 magnitude; Clark and Lauriol, 1992; Fig. 4), to be the result of the high-latitude setting that both sampling sites are located in. While existing CCC data is often biased towards central European/mid-latitude sites with isotopic compositions of $\text{CCC}_{\text{coarse}}$ and CCC_{fine} , plotting in distinct O and C ranges, our data demonstrates that such borders are not universally applicable, especially at higher latitudes.

300 Previous studies have shown that the $\delta^{18}\text{O}$ values of CCC_{fine} and common speleothems often overlap (Fig. 4; e.g., Luetscher et al., 2013; Žák et al., 2018), however, the $\delta^{18}\text{O}$ values of Cove Cave CCMs are more depleted than those of common speleothems from the same cave. While our data set is not sufficient to draw definite conclusions, we hypothesise that the isotopic composition of the source water, from which the CCMs and common speleothems precipitated, differed. While the CCMs precipitated recently from melted snow/ice (winter signal), the common speleothems formed from rainwater (annual or summer signal) during an earlier period within the Quaternary under different climatic boundary conditions.

305 This shift is also seen in CCC_{fine} from Canadian caves (Clark and Lauriol, 1992; Fig. 4), although at a smaller magnitude. There is also a difference between the $\delta^{18}\text{O}$ values of CCMs and (inactive) common speleothems from the same cave (-24 to -16 ‰ vs. -17 to -13 ‰ respectively), which is not in agreement with other CCC_{fine} -vs.-common speleothem studies, where the $\delta^{18}\text{O}$ values of CCC_{fine} either overlap with those of common speleothems or are slightly higher (Fig. 4; e.g., Luetscher et al., 2013; Žák et al., 2018).

310

5.3 Formation age

In this study, CCC_{fine} -fine-grained CCMs were successfully dated using both a U-Th isochron approach and ^{14}C dating with DCF correction. The isochron indicated that the ~~the~~ initial $^{230}\text{Th}/^{232}\text{Th}$ activity ratio (1.39 ± 0.006) was elevated in comparison to the bulk earth-derived value (i.e., 0.8; Wedepohl, 1995), which had therefore resulted in an under-correction for detrital Th (Table 1). For
315 dating CCC_{fine} -CCMs in this study, it is sufficient to solely use $^{230}\text{Th}/\text{U}$ methods but we also show that successful and reliable dating of fine-grained CCMs ~~CCC_{fine}~~ is possible using ^{14}C provided that the DCF can be constrained and corrected for. The independent age information, necessary for the DCF calculation, however, does not have to be provided by $^{230}\text{Th}/\text{U}$ dating; it could for instance come from ^{14}C dating of stratigraphically coeval organic matter. Where $^{230}\text{Th}/\text{U}$ dating of CCC_{fine} fine-grained CCMs is impracticable (e.g., due to low ^{238}U concentrations and/or high detrital Th contamination), ^{14}C dating could provide a viable
320 alternative. In this study, the ^{14}C dating results complement the $^{230}\text{Th}/\text{U}$ isochron age well. However, because the DCF-corrected ^{14}C age hits a plateau on the calibration curve (Reimer et al., 2020), the $^{230}\text{Th}/\text{U}$ method is considered a better approach in this study. On the other hand, ^{14}C dating of CCC_{fine} -fine-grained CCMs could be equally reliable as, or better than, $^{230}\text{Th}/\text{U}$ dating for

325 periods of time characterised by a steeply sloped calibration curve. Ultimately, the choice of dating will be study-dependent and
regardless of the method used, dating of [fine-grained CCMs](#) ~~CCC_{fine}~~ could provide additional chronological control on cave ice
bodies, an emerging (but rapidly disappearing) palaeoclimate archive (e.g., Kern and Perşoiu, 2013; Racine et al., 2022), in
particular in those settings [where organic inclusions are lacking](#).

5.4 Extreme event triggered CCM formation

330 High $\delta^{234}\text{U}_{\text{initial}}$ values suggest that the karst system of the cave was hydrologically inactive prior to the event that caused CCM
formation. During arid climate periods and/or under permafrost influence, ^{234}U accumulates in the crystal lattice of bedrock
minerals through alpha recoil and is easily mobilised when water becomes available (Fleischer, 1982). Speleothems, including
CCMs, may record this first mobilisation of ^{234}U after a period of accumulation by elevated $\delta^{234}\text{U}_{\text{initial}}$ values (e.g., Wendt et al.,
2020). The high $\delta^{234}\text{U}_{\text{initial}}$ of the Cove Cave CCMs (1872 ± 3 to 2193 ± 5) contrasts with the comparatively low $\delta^{234}\text{U}_{\text{initial}}$ of common
speleothems from the same cave, which represent a hydrologically active karst system (<150). The high $\delta^{234}\text{U}_{\text{initial}}$ of the Cove
335 Cave CCM therefore indicate a prolonged period of permafrost presence prior to their formation.

Combining the results of mineralogical analyses and dating, it can be concluded that the Cove Cave CCMs formed as a result of a
singular event at 65 ± 17 a BP (18859 ± 17 CE) and therefore during the cold climate of the late Little Ice Age (ca. 700-50 a BP;
Kjær et al., 2022). A reconstruction of surface temperature based on Greenland ice core data since 1840 CE indicates that the mid-
to late-1880s CE ($65-60$ a BP) were some of the coolest years on record (Box et al., 2009). It can therefore be assumed that the
340 climate of northeast Greenland during the time of CCM formation was colder and permafrost was more abundant than today. In
order for ~~the~~ water to enter the cave through the frozen rock and not immediately freeze and [sublimate](#) on the walls, it must carry
enough latent heat. Any event that led to these conditions in and around Cove Cave must have been anomalous, which is supported
by the lack of CCMs observed in other caves of the area [\(based on the findings of two expeditions that were part of this project\)](#).

345 In order to explain the formation of fine-grained CCMs in Cove Cave, we consider the following scenarios: i) an extreme rainfall
event providing enough water and thus latent heat to enter Cove Cave; ii) migration of the hoar frost boundary and melt pond
deeper into the cave due to the influx of warm and moist air; iii) an increase of the active layer thickness of (wet) permafrost due
to an anomalously warm summer/year/interval; iv) higher cave air temperatures and water availability due to temperate ice covering
the cave; and v) enhanced melting of the local ice cap.

350 There is no evidence for (i) an extreme rainfall event in the high-resolution Greenland ice cores during the time of CCM formation,
although it cannot be excluded that such an event occurred locally or regionally. Though a tectonic fracture exists in the roof of
Cove Cave, which could promote water infiltration, the lack of CCM formation in other caves of the area renders this scenario
unlikely. Furthermore, in this arid region with ca. 200 mm per year of precipitation (Schuster et al., 2021), extreme rainfall events
with high volumes of water do not occur. Scenario (ii) seems unlikely as the hoar frost boundary is located at the high point in
Cove Cave (Fig. 2). Such boundaries are only observed at the highest points in the Greenland Caves (Barton et al., 2020), hence
355 shifting this boundary deeper into the cave is unlikely to occur based on the sag-type geometry of the cave, which determines the
location of the cold pool interface. An unusually warm summer/year/interval that could potentially lead to (iii) an increase of active
layer thickness would have been recorded by Greenland ice cores as well as observational records along the coast of south and
west Greenland. Based on a merged south-west Greenland temperature record (Vinther et al., 2006), there is no
summer/year/interval that stands out as being particularly warm in the period of 1868-1902 CE (i.e., 65 ± 17 a BP). Another

360 argument against scenario (iii) is, again, the lack of CCMs in other caves in the area. While it is very likely that an ice cap covered
the plateau above Cove Cave in the time interval of interest (Fig. 1), scenario (iv) fails to explain why there was only one generation
of CCMs found in Cove Cave, since higher cave air temperatures and water availability would probably have lasted for a prolonged
interval. The ice cap does, however, appear to be a key factor together with a tectonic fracture in the roof of the cave, as they enable
a mechanism in which sufficient water can pass through the permafrost and enter the underground. Specifically, enhanced melting
365 of the local ice cap (v) could have been triggered by anomalously high temperatures and concurrent lowering of the albedo due to
black carbon deposition. Both of these factors have been recognised as the cause for ice-melting conditions all over the Greenland
ice sheet, including the dry snow zone, in 1889 CE (Clausen et al., 1988; Fischer et al., 1998; Keegan et al., 2014; Neff et al.,
2014). This event is often referred to as the “summer melt episode” of 1889 CE, which, according to Neff et al. (2014), lasted for
a few days. ~~that lasted a few days (Neff et al., 2014) and concurrent lowering of the albedo due to black carbon deposition on the~~
370 ~~ice cap. This combination of factors led to ice melting conditions all over the Greenland ice sheet in 1889 CE (Clausen et al., 1988;
Fischer et al., 1998; Keegan et al., 2014; Neff et al., 2014), which is often referred to as the “summer melt episode” of 1889 CE.~~
This episode—the summer melt episode occurred synchronously within dating uncertainty with the timing of the CCM formation
(1885 CE; 65±17 a BP). Closer to our study site, an ice core from the Flade Isblink ice cap recorded a warming between 1920–
1930 CE (30–20 a BP) as increased melt percentage, but it did not record enhanced melt during 1889 CE, which might simply be
375 the result of a non-definitive time scale that does not allow for the investigation of short-term events (Lemark, 2010). The ice core
from Flade Isblink did, however, record a high concentration of black carbon in 1889 CE (Eckhardt et al., 2023). Nevertheless,
we therefore infer that the unusually high air temperatures and black carbon deposition associated with this event affected our
study area as well, leading to enhanced melting of the local ice cap, with more water entering moulines, reaching the base of the ice
cap, and then finding its way through conduits, possibly through tectonic fractures, into the cave. This water turned to ice in the
380 heavily undercooled cave resulting in the precipitation of ~~CCC_{fine}~~ fine-grained cryogenic cave carbonates and potentially also
cryogenic gypsum during a rather rapid freezing process. Subsequently, the ice sublimated in the cold and dry microclimate of the
cave releasing enclosed ~~CCC_{fine} and~~ cryogenic calcite and gypsum particles which accumulated on the cave floor. As discussed
above, the origin of the other hydrous sulphate minerals is less clear; they were, however, found intermixed with calcite-CCC_{fine}
and gypsum in the same spot, hinting towards a near-synchronous formation.

385 The presence of CCMs in Cove Cave indicate that the conditions leading to the summer melt episode of 1889 CE also reached
further northeast and thus affected the area surrounding the cave. Linking the CCM formation to this short-term extreme event
further provides hints about the rate of formation of fine-grained CCMs (which is a highly understudied field), while demonstrating
why fine-grained CCMs cannot be used as a permafrost proxy as the presence or absence of permafrost is generally not influenced
by short-term weather conditions.

390

6 Conclusions

Fine-grained CCMs from Cove Cave, a low-elevation, high-latitude permafrost cave in northeast Greenland, consist of an unusual
mixture of minerals: cryogenic calcite (~~CCC_{fine}~~), potentially cryogenic gypsum, and other hydrous sulphate minerals (eugsterite,
mirabilite, löweite), whose mode of formation is less clear but presumably at least associated with cryochemical processes and/or
395 subsequent sublimation of the ice body in a dry cave atmosphere. The high solubility of the sulphate minerals suggests that since
their formation, and after the sublimation of ice, the microclimate at the sampling site has remained cold, dry, and ice-free, as it is
today.

400 The Greenland CCMs extend the knowledge of the stable isotopic composition of CCMs. While their $\delta^{13}\text{C}$ values are comparable to those of mid-latitude CCC_{fine} , the $\delta^{18}\text{O}$ values are lower compared to both common (inactive) speleothems from the same cave and CCC_{fine} from the mid-latitudes. These lower $\delta^{18}\text{O}$ values can be attributed to much lower $\delta^{18}\text{O}$ values of meteoric precipitation in the high latitudes and, to a lesser extent, the difference in the isotopic composition of the water sources during the formation of CCMs and common speleothems.

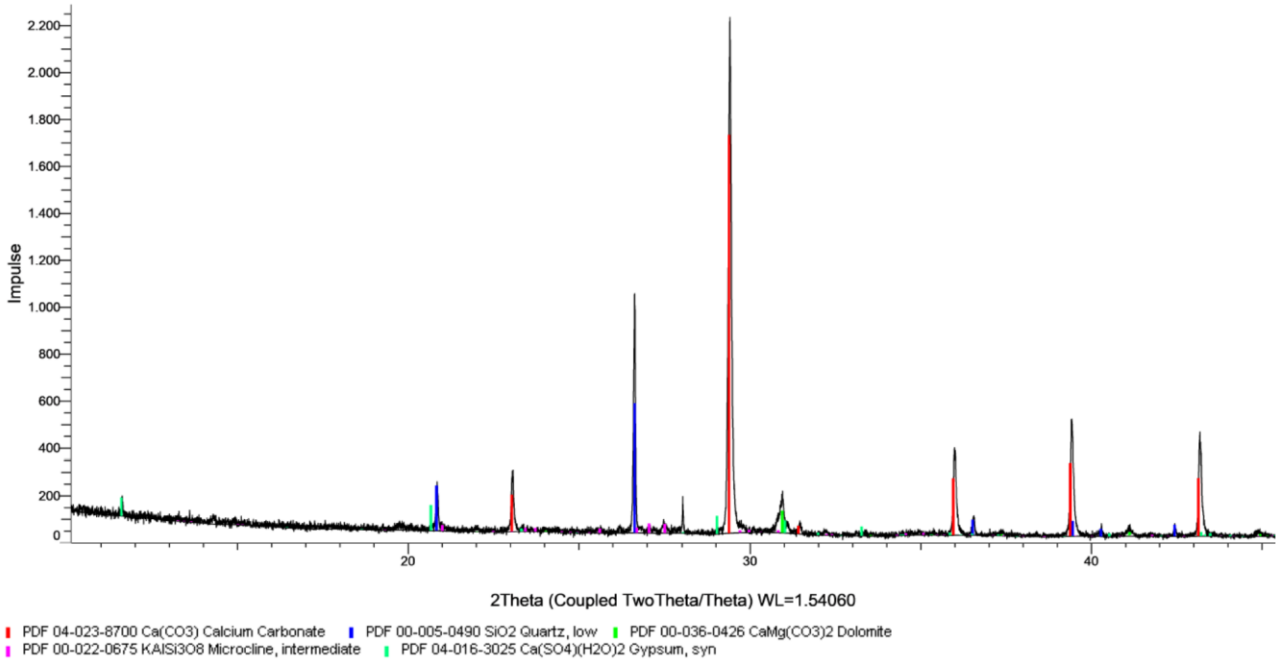
405 We show that precise dating of [fine-grained CCMs, and hence \$\text{CCC}_{\text{fine}}\$](#) is in principle possible with $^{230}\text{Th}/\text{U}$ or ^{14}C dating. Using isochrons and a site-specific initial $^{230}\text{Th}/^{232}\text{Th}$ correction factor is paramount for accurate $^{230}\text{Th}/\text{U}$ ages. In this study, $^{230}\text{Th}/\text{U}$ is arguably superior to ^{14}C dating, which is dependent on the slope of a calibration curve and independent age information to constrain the DCF. However, its application is restricted to samples of low detrital Th content (and rather high U concentration). Where these conditions cannot be met, ^{14}C dating might be a better alternative. The possibility to date [\$\text{CCC}_{\text{fine}}\$ -fine-grained CCMs](#) with either $^{230}\text{Th}/\text{U}$ or ^{14}C could aid the establishment of reliable chronologies for cave ice as a palaeoclimate archive.

410 We conclude that CCM formation in Cove Cave was most likely the result of a single [short-term](#) extreme event [that also led leading](#) to the summer melt episode of 1889 CE on the Greenland ice sheet, [which-causing-also-caused](#) enhanced melting on the local ice cap on the plateau above the cave. [The Cove Cave CCMs therefore give an indication regarding the spatial extent of melting conditions in an area outside of the Greenland ice sheet, while also providing hints about the rate of CCM formation.](#)

[Appendix A: Supplementary information on XRD analysis](#)

415 [XRD analyses were conducted in two laboratories during different stages of the project. The displayed X-ray diffractograms show the results of one of the laboratories at a later stage in the project. While the results between the labs were mostly comparable, mirabilite was found during analysis of KC19CCC-2 and -3 ~~in~~at an early stage of the project. This result could not be replicated during analysis later in the project. We attribute this inconsistency to imperfect homogenisation of the samples prior to analyses, which might have been enhanced by the small sample volumes required for XRD analysis.](#)

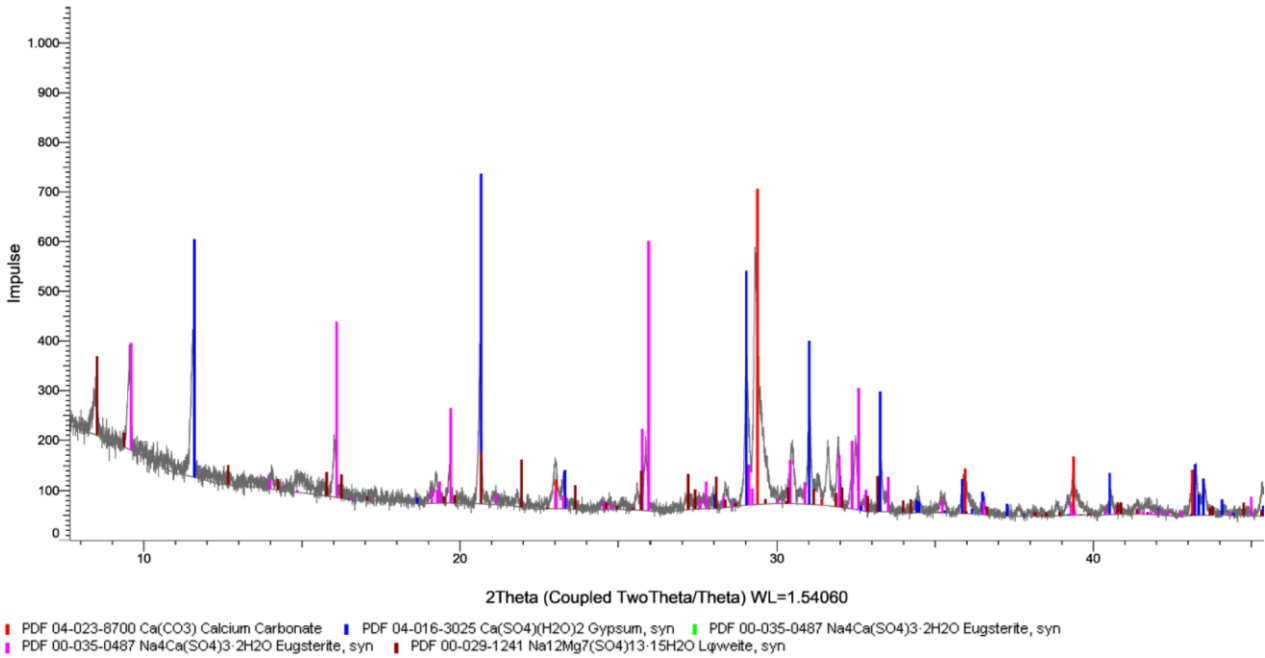
KC19CCC-1



420

Figure A1: X-ray diffractogram of sample KC19CCC-1. This sample contains calcite, gypsum, quartz, dolomite, and potassium feldspar.

KC19CCC-2



425

Figure A2: X-ray diffractogram of sample KC19CCC-2. As displayed, this sample contains calcite, gypsum, eugsterite, and löweite. During XRD analysis in another laboratory, mirabilite was also found in the sample.

KC19CCC-3

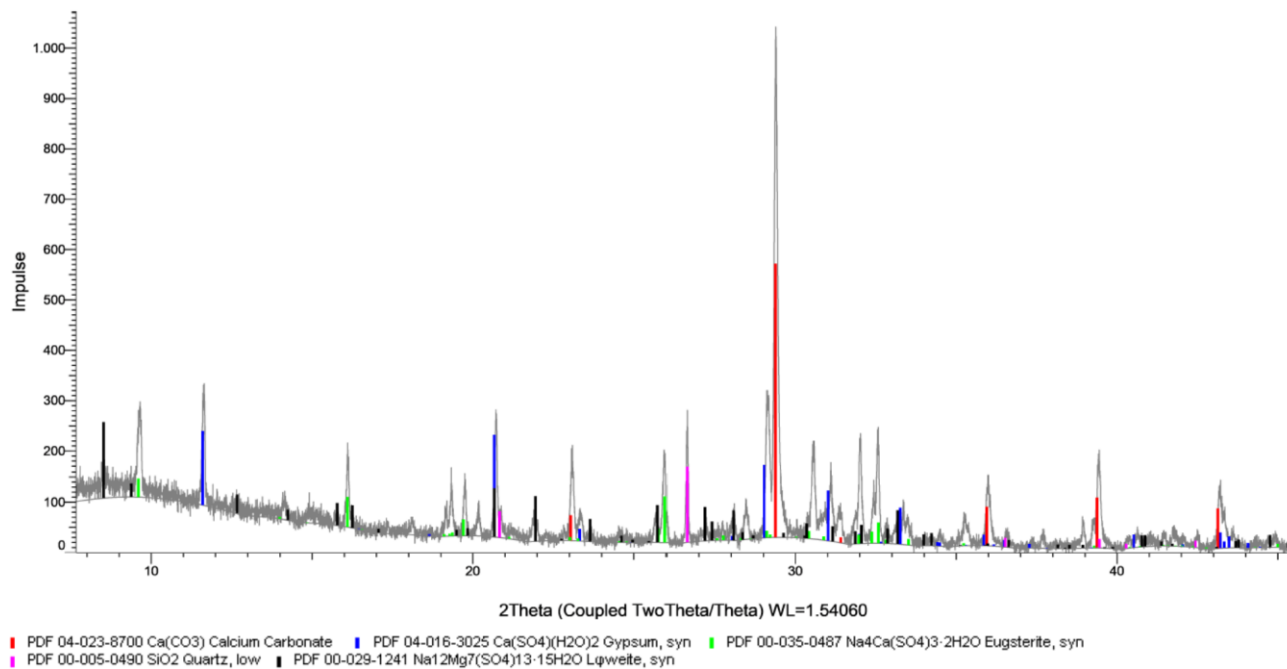


Figure A3: X-ray diffractogram of sample KC19CCC-3, also representative for KC19CCC-4. As shown, this sample contains calcite, gypsum, eugsterite, löweite, and quartz. During XRD analysis in another laboratory, mirabilite was also detected.

430

Competing interests

The authors declare that they have no conflict of interest.

Author contribution

435 AD designed the methodology, interpreted the data, and wrote the paper. PT assisted with field work, age calculations, and manuscript preparation. CS assisted with analyses, contributed to discussions and manuscript preparation. IH performed ^{14}C dating. XL contributed with $^{230}\text{Th}/\text{U}$ disequilibrium analyses. RLE provided analytical $^{230}\text{Th}/\text{U}$ disequilibrium dating facilities. GEM (P. I.) designed the study, raised the funding, organised, led and participated in the fieldwork, contributed to the discussions and manuscript preparation.

440

Acknowledgements

We thank Manuela Wimmer for stable isotope measurements, Clivia Hejny for XRD analyses, Kristian Pfaller for SEM images, Andreas Saxer for XRD analyses and SEM images, and Bastian Joachim-Mrosko for Raman spectroscopy. We are grateful to Hazel Barton, Chris Blakeley, Pete Hodkinson, Adam Ignézi, Robbie Shone, Paul Smith, and Andrew Sole, who participated in
445 the 2019 Greenland Caves Expedition. This research has been supported by the Austrian Science Fund (FWF) project no. Y 1162N37 to Gina E. Moseley. Data from the Programme for Monitoring of the Greenland Ice Sheet (PROMICE) were provided by the Geological Survey of Denmark and Greenland (GEUS) at <http://www.promice.dk>. The Greenland government are thanked

450

References

- Audra, P. and Nobécourt, J.-C.: Rare sulfates (mirabilite, eugsterite) in the dry microclimate of chamois cave (Alpes-de-Haute-Provence, France), in: Proceedings of the 16th International Congress of Speleology, Czech Speleological Society, Prague, Czech Republic, 21-28 July 2013, 432–436, 2013.
- 455 Bajo, P., Borsato, A., Drysdale, R., Hua, Q., Frisia, S., Zanchetta, G., Hellstrom, J., and Woodhead, J.: Stalagmite carbon isotopes and dead carbon proportion (DCP) in a near-closed-system situation: An interplay between sulphuric and carbonic acid dissolution, *Geochim. Cosmochim. Ac.*, 210, 208–227, <https://doi.org/10.1016/j.gca.2017.04.038>, 2017.
- Bartolomé, M., Sancho, C., Osácar, M. C., Moreno, A., Leunda, M., Spötl, C., Luetscher, M., López-Martínez, J., and Belmonte, A.: Characteristics of cryogenic carbonates in a Pyrenean ice cave (northern Spain), *Geogaceta*, 58, 107–110, 2015.
- 460 Bartolomé, M., Cazenave, G., Luetscher, M., Spötl, C., Gázquez, F., Belmonte, Á., Turchyn, A. V., López-Moreno, J. I., and Moreno, A.: Mountain permafrost in the Central Pyrenees: insights from the Devaux ice cave, *EGUosphere Discussions* [preprint], <https://doi.org/10.5194/egusphere-2022-349>, 17 May 2022.
- Barton, H. A., Breley, G. J., Töchterle, P., and Moseley, G. E.: Cryogenic features of the permafrost ice caves of Grottedal, northeast Greenland, *Cave and Karst Science*, 47, 93–99, 2020.
- 465 Bieniok, A., Zagler, G., Brendel, U., and Neubauer, F.: Speleothems in the dry cave parts of the Gamslöcher-Kolowrat Cave, Untersberg near Salzburg (Austria), *Int. J. Speleol.*, 40, 117-124, 2011.
- Bintanja, R. and Krikken, F.: Magnitude and pattern of Arctic warming governed by the seasonality of radiative forcing, *Sci. Rep-UK*, 6, 1-7, <https://doi.org/10.1038/srep38287>, 2016.
- Bintanja, R. and Selten, F. M.: Future increases in Arctic precipitation linked to local evaporation and sea-ice retreat, *Nature*, 470, 479–482, <https://doi.org/10.1038/nature13259>, 2014.
- Box, J. E., Yang, L., Bromwich, D. H., and Bai, L.-S.: Greenland Ice Sheet surface air temperature variability: 1840–2007*, *J. Climate*, 22, 4029–4049, <https://doi.org/10.1175/2009JCLI2816.1>, 2009.
- Bronk Ramsey, C.: Bayesian analysis of radiocarbon dates, *Radiocarbon*, 51, 337–360, <https://doi.org/10.1017/S0033822200033865>, 2009.
- 475 Cheng, H., Edwards, R. L., Shen, C.-C., Polyak, V. J., Asmerom, Y., Woodhead, J., Hellstrom, J., Wang, Y., Kong, X., Spötl, C., Wang, X., and Alexander Jr., E. C.: Improvements in ^{230}Th dating, ^{230}Th and ^{234}U half-life values, and U–Th isotopic measurements by multi-collector inductively coupled plasma mass spectrometry, *Earth Planet Sc. Lett.*, 371-372, 82-91, <https://doi.org/10.1016/j.epsl.2013.04.006>, 2013.
- Clark, I.D. and Lauriol, B.: Kinetic enrichment of stable isotopes in cryogenic calcites, *Chem. Geol.*, 102, 217–228, [https://doi.org/10.1016/0009-2541\(92\)90157-Z](https://doi.org/10.1016/0009-2541(92)90157-Z), 1992.
- 480 Clausen, H. B., Gundestrup, N. S., Johnsen, S. J., Bindschadler, R., and Zwally, J.: Glaciological investigations in the Crête area, central Greenland: A search for a new deep-drilling site, *Ann. Glaciol.*, 10, 10–15, <https://doi.org/10.3189/S0260305500004080>, 1988.
- 485 Dahl-Jensen, D., Mosegaard, K., Gundestrup, N., Clow, G. D., Johnsen, S. J., Hansen, A. W., and Balling, N.: Past temperatures directly from the Greenland ice sheet, *Science*, 282, 268–271, <https://doi.org/10.1126/science.282.5387.268>, 1998.
- Danmarks Meteorologiske Institut: Klimanormaler for Grønland [dataset], <https://www.dmi.dk/vejrkarkiv/normaler-gronland/>, last access: July 12, 2022.
- Davies, W. E. and Krinsley, D. B.: Caves in Northern Greenland, *National Speleol. Soc. Bull.*, 22, 114–116, 1960.
- Donner, A., Töchterle, P., and Moseley, G. E.: Basic meteorological observations in the Centrumso region of northeast Greenland, *Cave and Karst Science*, 47, 104–106, 2020.
- 490 Dorale, J. A., Edwards, R. L., Alexander, E. C., Shen, C.-C., Richards, D. A., and Cheng, H.: Uranium-series dating of speleothems: current techniques, limits, & applications, in: *Studies of Cave Sediments*, edited by: Sasowsky, I. D. and Mylroie, J., Springer US, Boston, MA, 177–197, https://doi.org/10.1007/978-1-4419-9118-8_10, 2004.
- Dublyansky, Y., Kadebskaya, O., Menshikova, E., Demeny, A., and Spötl, C.: Polymicrobial cryogenic deposits in caves of the Southern Ural, Russia, as tracers of past permafrost, in: *Climate Change: The Karst Record 8th International Conference*, Scientific Program and Abstracts, Austin, USA, 21-24 May 2017, 46, 2017.
- [Eckhardt, S., Pisso, I., Evangelidou, N., Zwaafink, C. G., Plach, A., McConnell, J. R., Sigl, M., Ruppel, M., Zdanowicz, C., Lim, S., Chellman, N., Opel, T., Meyer, H., Steffensen, J. P., Schwikowski, M., and Stohl, A.: Revised historical Northern](#)

- 500 [Hemisphere black carbon emissions based on inverse modelling of ice core records, Nat. Commun., 14, 217, https://doi.org/10.1038/s41467-022-35660-0, 2023.](https://doi.org/10.1038/s41467-022-35660-0)
- Edwards, R. L., Chen, J. H., and Wasserburg, G. J.: ^{238}U - ^{234}U - ^{230}Th - ^{232}Th systematics and the precise measurement of time over the past 500,000 years, *Earth Planet. Sc. Lett.*, 81, 175–192, [https://doi.org/10.1016/0012-821X\(87\)90154-3](https://doi.org/10.1016/0012-821X(87)90154-3), 1987.
- Fausto, R. S., van As, D., and Mankoff, K. D.: Programme for monitoring of the Greenland ice sheet (PROMICE): Automatic weather station data, Version: v03 [data set], Geological survey of Denmark and Greenland (GEUS),
505 <https://doi.org/10.22008/promice/data/aws>, 2019.
- Fischer, H., Werner, M., Wagenbach, D., Schwager, M., Thorsteinsson, T., Wilhelms, F., Kipfstuhl, J., and Sommer, S.: Little Ice Age clearly recorded in northern Greenland ice cores, *Geophys. Res. Lett.*, 25, 1749–1752,
<https://doi.org/10.1029/98GL01177>, 1998.
- Fleischer, R. L.: Alpha-recoil damage and solution effects in minerals: uranium isotopic disequilibrium and radon release,
510 *Geochim. Cosmochim. Ac.*, 46, 2191–2201, [https://doi.org/10.1016/0016-7037\(82\)90194-6](https://doi.org/10.1016/0016-7037(82)90194-6), 1982.
- Genty, D. and Massault, M.: Bomb ^{14}C recorded in laminated speleothems: calculation of dead carbon proportion, *Radiocarbon*, 39, 33–48, <https://doi.org/10.1017/S0033822200040881>, 1997.
- Geofabrik and OpenStreetMap Contributors: <https://download.geofabrik.de/north-america/greenland-latest-free.shp.zip> [data set], 2018.
- 515 Harmon, R.S., Atkinson, T.C. and Atkinson, J.L.: The mineralogy of Castleguard Cave, Columbia Icefields, Alberta, Canada, *Arctic Alpine Res.*, 15, 503-516, 1983.
- Hajdas, I., Ascough, P., Garnett, M. H., Fallon, S. J., Pearson, C. L., Quarta, G., Spalding, K. L., Yamaguchi, H., and Yoneda, M.: Radiocarbon dating, *Nat. Rev. Methods Primers* 1, <https://doi.org/10.1038/s43586-021-00058-7>, 2021.
- Hill, C., and Forti, P.: *Cave Minerals of the World*. 2nd ed., Huntsville, National Speleological Society, 1997.
- 520 Hua, Q., McDonald, J., Redwood, D., Drysdale, R., Lee, S., Fallon, S., and Hellstrom, J.: Robust chronological reconstruction for young speleothems using radiocarbon, *Quat. Geochronol.*, 14, 67–80, <https://doi.org/10.1016/j.quageo.2012.04.017>, 2012.
- Jaffey, A. H., Flynn, K. F., Glendenin, L. E., Bentley, W. C., and Essling, A. M.: Precision measurement of half-lives and specific activities of ^{235}U and ^{238}U , *Phys. Rev. C*, 4, 1889-1906, <https://doi.org/10.1103/PhysRevC.4.1889>, 1971.
- 525 Kadebskaya, O., and Tschaiikovskiy, I.: Staging in the hypergene transformation of sulphate and carbonate rocks (based on slide-rocks under organ tubes in Kungur ice cave), *Acta Carsologica*, 44, 237-250, 2015.
- Keegan, K. M., Albert, M. R., McConnell, J. R., and Baker, I.: Climate change and forest fires synergistically drive widespread melt events of the Greenland Ice Sheet, *P. Natl. Acad. Sci. USA*, 111, 7964–7967, <https://doi.org/10.1073/pnas.1405397111>, 2014.
- 530 Kern, Z. and Perşoiu, A.: Cave ice – the imminent loss of untapped mid-latitude cryospheric palaeoenvironmental archives, *Quat. Sci. Rev.*, 67, 1–7, <https://doi.org/10.1016/j.quascirev.2013.01.008>, 2013.
- Kjær, K. H., Bjørk, A. A., Kjeldsen, K. K., Hansen, E. S., Andresen, C. S., Siggaard-Andersen, M.-L., Khan, S. A., Søndergaard, A. S., Colgan, W., Schomacker, A., Woodroffe, S., Funder, S., Rouillard, A., Jensen, J. F., and Larsen, N. K.: Glacier response to the Little Ice Age during the Neoglacial cooling in Greenland, *Earth-Sci. Rev.*, 227, 1-43,
535 <https://doi.org/10.1016/j.earscirev.2022.103984>, 2022.
- Koltai, G., Spötl, C., Jarosch, A.H., and Cheng, H.: Cryogenic cave carbonates in the Dolomites (northern Italy): insights into Younger Dryas cooling and seasonal precipitation, *Clim. Past*, 17, 775–789, <https://doi.org/10.5194/cp-17-775-2021>, 2021.
- Lacelle, D., Lauriol, B., and Clark, I. D.: Formation of seasonal ice bodies and associated cryogenic cave carbonates in Caverne de L'Ours, Québec, Canada: Kinetic isotope effects and pseudo-biogenic crystal structures, *J. Cave Karst Stud.*, 71, 48–62,
540 2009.
- Lauriol, B., Carrier, L., and Thibaudeau, P.: Topoclimatic zones and ice dynamics in the caves of the Northern Yukon, Canada, *Arctic*, 41, 215–220, <http://www.jstor.org/stable/40510717>, 1988.
- Lauriol, B. and Clark, I. D.: An approach to determine the origin and age of massive ice blockages in two arctic caves, *Permafrost Periglac.*, 4, 77–85, <https://doi.org/10.1002/ppp.3430040107>, 1993.
- 545 Lemark, A.: A study of the Flade Isblink ice cap using a simple ice flow model, Master thesis, Niels Bohr Institute Copenhagen University, Centre for Ice and Climate, Denmark, 75 pp., 2010.
- Loubière, J.-F.: Observations préliminaires sur les cavités de la région du lac Centrum (NE Groenland), *Karstologia: revue de karstologie et de spéléologie physique*, 9, 7–16, <https://doi.org/10.3406/karst.1987.2152>, 1987.
- Ludwig, K. R. and Titterton, D. M.: Calculation of $^{230}\text{Th}/\text{U}$ isochrons, ages, and errors. *Geochim. Cosmochim. Ac.*, 58, 5031–5042, [https://doi.org/10.1016/0016-7037\(94\)90229-1](https://doi.org/10.1016/0016-7037(94)90229-1), 1994.
- 550 Luetscher, M., Borreguero, M., Moseley, G. E., Spötl, C., and Edwards, R. L.: Alpine permafrost thawing during the Medieval Warm Period identified from cryogenic cave carbonates, *Cryosphere*, 7, 1073–1081, <https://doi.org/10.5194/tc-7-1073-2013>, 2013.

- 555 Moseley, G. E., Barton, H. A., Spötl, C., Töchterle, P., Smith, M. P., Bjerkenås, S. E., Blakely, C., Hodkinson, P. D., Shone, R. C., Sivertsen, H. C., and Wright, M.: Cave discoveries and speleogenetic features in northeast Greenland, *Cave and Karst Science*, 47, 74–87, 2020.
- Moseley, G. E., Edwards, R. L., Lord, N. S., Spötl, C., and Cheng, H.: Speleothem record of mild and wet mid-Pleistocene climate in northeast Greenland, *Sci. Adv.*, 7, <https://doi.org/10.1126/sciadv.abe1260>, 2021.
- 560 Neff, W., Compo, G. P., Ralph, F. M., and Shupe, M. D.: Continental heat anomalies and the extreme melting of the Greenland ice surface in 2012 and 1889, *J. Geophys. Res.-Atmos.*, 119, 6520–6536, <https://doi.org/10.1002/2014JD021470>, 2014.
- Racine, T. M. F., Reimer, P. J., and Spötl, C.: Multi-centennial mass balance of perennial ice deposits in Alpine caves mirrors the evolution of glaciers during the Late Holocene, *Sci. Rep.-UK*, 12, 1–13, <https://doi.org/10.1038/s41598-022-15516-9>, 2022.
- Reimer, P. J., Brown, T. A., and Reimer, R. W.: Discussion: Reporting and calibration of post-bomb ^{14}C data, *Radiocarbon*, 46, 1299–1304, <https://doi.org/10.1017/S0033822200033154>, 2004.
- 565 Reimer, P. J., Austin, W. E. N., Bard, E., Bayliss, A., Blackwell, P. G., Bronk Ramsey, C., Butzin, M., Cheng, H., Edwards, R. L., Friedrich, M., Grootes, P. M., Guilderson, T. P., Hajdas, I., Heaton, T. J., Hogg, A. G., Hughen, K. A., Kromer, B., Manning, S. W., Muscheler, R., Palmer, J. G., Pearson, C., van der Plicht, J., Reimer, R. W., Richards, D. A., Scott, E. M., Southon, J. R., Turney, C. S. M., Wacker, L., Adolphi, F., Büntgen, U., Capano, M., Fahrni, S. M., Fogtmann-Schulz, A., Friedrich, R., Köhler, P., Kudsk, S., Miyake, F., Olsen, J., Reinig, F., Sakamoto, M., Sookdeo, A., and Talamo, S.: The IntCal20 Northern Hemisphere radiocarbon age calibration curve (0–55 cal kBP), *Radiocarbon*, 62, 725–757, <https://doi.org/10.1017/RDC.2020.41>, 2020.
- Rhodes, R. H., Yang, X., and Wolff, E. W.: Sea ice versus storms: What controls sea salt in Arctic ice cores?, *Geophys. Res. Lett.*, 45, 5572–5580, <https://doi.org/10.1029/2018GL077403>, 2018.
- 575 Richter, D. K., Scholz, D., Jöns, N., Neuser, R. D., and Breitenbach, S. F.: Coarse-grained cryogenic aragonite as end-member of mineral formation in dolomite caves, *Sediment. Geol.*, 376, 136–146, <https://doi.org/10.1016/j.sedgeo.2018.08.006>, 2018.
- Schuster, L., Maussion, F., Langhamer, L., and Moseley, G. E.: Lagrangian detection of precipitation moisture sources for an arid region in northeast Greenland: relations to the North Atlantic Oscillation, sea ice cover, and temporal trends from 1979 to 2017, *Weather Clim. Dynam.*, 2, 1–17, <https://doi.org/10.5194/wcd-2-1-2021>, 2021.
- 580 Shen, C.-C., Wu, C.-C., Cheng, H., Edwards, R. L., Hsieh, Y.-T., Gallet, S., Chang, C.-C., Li, T.-Y., Lam, D. D., Kano, A., Hori, M., and Spötl, C.: High-precision and high-resolution carbonate ^{230}Th dating by MC-ICP-MS with SEM protocols, *Geochim. Cosmochim. Ac.*, 99, 71–86, <https://doi.org/10.1016/j.gca.2012.09.018>, 2012.
- Shepherd, T. G.: Effects of a warming Arctic, *Science*, 353, 989–990, <https://doi.org/10.1126/science.aag2349>, 2016.
- Smith, M. P. and Rasmussen, J. A.: The geology of the Centrumso area of Kronprins Christian Land, northeast Greenland, and lithological constraints on speleogenesis, *Cave and Karst Science*, 47, 60–65, 2020.
- 585 Sole, A. J., Ignéczi, Á., Smith, M. P., and Clark, C. D.: Investigations to constrain retreat of the Greenland Ice Sheet: glacial geomorphology and sampling for cosmogenic exposure dating of the Centrumso area, Kronprins Christian Land, northeast Greenland, *Cave and Karst Science*, 47, 66–73, 2020.
- Spötl, C.: Kryogene Karbonate im Höhleneis der Eisriesenwelt, *Die Höhle*, 59, 26–36, 2008.
- 590 Spötl, C.: Long-term performance of the Gasbench isotope ratio mass spectrometry system for the stable isotope analysis of carbonate microsamples, *Rapid Commun. Mass. Spectrom.*, 25, 1683–1685, <https://doi.org/10.1002/rcm.5037>, 2011.
- Spötl, C. and Cheng, H.: Holocene climate change, permafrost and cryogenic carbonate formation: insights from a recently deglaciated, high-elevation cave in the Austrian Alps, *Clim. Past*, 10, 1349–1362, <https://doi.org/10.5194/cp-10-1349-2014>, 2014.
- 595 Spötl, C., Koltai, G., Jarosch, A. H., and Cheng, H.: Increased autumn and winter precipitation during the Last Glacial Maximum in the European Alps, *Nature Commun.*, 12, <https://doi.org/10.1038/s41467-021-22090-7>, 2021.
- Spötl, C. and Vennemann, T. W.: Continuous-flow isotope ratio mass spectrometric analysis of carbonate minerals, *Rapid Commun. Mass Sp.*, 9, 1004–1006, <https://doi.org/10.1002/rcm.1010>, 2003.
- Stuiver, M. and Polach, H. A.: Discussion reporting of ^{14}C data, *Radiocarbon*, 19, 355–363, <https://doi.org/10.1017/S0033822200003672>, 1997.
- 600 Synal, H.-A., Stocker, M., and Suter, M.: MICADAS: A new compact radiocarbon AMS system, *Nucl. Instrum. Meth. B*, 259, 7–13, <https://doi.org/10.1016/j.nimb.2007.01.138>, 2007.
- Töchterle, P., Steidle, S., Edwards, R. L., Dublyansky, Y., Spötl, C., Li, X., Gunn, J., and Moseley, G. E.: $^{230}\text{Th}/\text{U}$ isochron dating of cryogenic cave carbonates, *Geochronology*, 4, 617–627, <https://doi.org/10.5194/gchron-4-617-2022>, 2022.
- 605 van As, D., Fausto, R. S., Ahlström, A. P., Andersen, S. B., Andersen, M. L., Citterio, M., Edolvang, K., Gravesen, P., Machguth, H., Nick, F. M., Nielsen, S., and Weidick, A.: Programme for monitoring of the Greenland Ice Sheet (PROMICE): first temperature and ablation records, *Geol. Surv. Den. Greenl.*, 23, 73–76, <https://doi.org/10.5167/uzh-131209>, 2011.
- Vermeesch, P.: IsoplotR: A free and open toolbox for geochronology, *Geosci. Front*, 9, 1479–1493, <https://doi.org/10.1016/j.gsf.2018.04.001>, 2018.

- 610 Vinther, B. M., Andersen, K. K., Jones, P. D., Briffa, K. R., and Cappelen, J.: Extending Greenland temperature records into the late eighteenth century, *J. Geophys. Res.*, 111, D11105, <https://doi.org/10.1029/2005JD006810>, 2006.
- Wedepohl, K. H.: The composition of the continental crust, *Geochim. Cosmochim. Ac.*, 59, 1217–1232, [https://doi.org/10.1016/0016-7037\(95\)00038-2](https://doi.org/10.1016/0016-7037(95)00038-2), 1995.
- 615 Wendt, K. A., Pythoud, M., Moseley, G. E., Dublyansky, Y. V., Edwards, R. L., and Spötl, C.: Paleohydrology of southwest Nevada (USA) based on groundwater $^{234}\text{U}/^{238}\text{U}$ over the past 475 k.y., *Geol. Soc. Am. Bull.*, 132, 793–802, <https://doi.org/10.1130/B35168.1>, 2020.
- White, W. B.: Mineralogy of Mammoth Cave, in: *Mammoth Cave*, edited by: Hobbs III, H. H., Olson, R. A., Winkler, E. G., and Culver, D. C., Springer, Cham, 145–162, https://doi.org/10.1007/978-3-319-53718-4_9, 2017.
- 620 Žák, K., Richter, D. K., Filippi, M., Živor, R., Deininger, M., Mangini, A., and Scholz, D.: Coarsely crystalline cryogenic cave carbonate – a new archive to estimate the Last Glacial minimum permafrost depth in Central Europe, *Clim. Past*, 8, 1821–1837, <https://doi.org/10.5194/cp-8-1821-2012>, 2012.
- Žák, K., Onac, B.P., Kadebskaya, O.I., Filippi, M., Dublyansky, Y., and Luetscher, M.: Cryogenic mineral formation in caves, in: *Ice Caves*, edited by: Perşoiu, A. and Lauritzen, S.-E., Elsevier, Amsterdam, Netherlands, 123–162, <https://doi.org/10.1016/B978-0-12-811739-2.00035-8>, 2018.

625